DOI:10.11973/jxgccl240514

焊枪摆动幅度对304L不锈钢补强板TIG焊接接头组织和性能的影响

朱加雷[1],朱文磊[1],焦向东[1],李守根[1],郭方涛[1],张洪涛[2]
(1. 北京石油化工学院机械工程学院,北京 102617;2. 哈尔滨工业大学(威海)材料科学与工程学院,威海 264209)

摘 要:选用ER316L焊丝,采用自动钨极惰性气体保护(TIG)焊结合摆动焊接技术,在焊枪不同摆动幅度(2,3,4 mm)下对304L不锈钢进行补强板焊接试验,研究了摆动幅度对接头焊缝显微组织、物相组成、显微硬度和耐腐蚀性能的影响。结果表明:不同摆动幅度下接头焊缝的组织主要由γ-奥氏体和δ-铁素体组成;随着摆动幅度增加,γ相(111)晶面衍射峰强度降低,δ相(110)晶面衍射峰强度增加,较大摆动幅度(3,4 mm)下δ-铁素体以骨架状沿γ-奥氏体柱状晶/等轴晶的晶界分布。随着摆动幅度增加,由于δ-铁素体含量增加、γ-奥氏体含量减少且晶粒细化,焊缝硬度提高,自腐蚀电位减小,自腐蚀电流密度增大,耐腐蚀性能降低。

关键词:钨极惰性气体保护焊;摆动焊接;304L不锈钢;显微组织;电化学腐蚀
中图分类号:TG444.74 **文献标志码**:A **文章编号**:1000-3738(2025)08-0015-04

0 引 言

304L不锈钢具有优异的耐腐蚀性能、耐热性、耐微酸性和良好的力学性能、加工性能等,广泛应用于核电站关键设备(如第二代核电站乏燃料水池)[1-3],但在服役过程中会因长期处于含特定离子的水介质环境而发生局部腐蚀甚至开裂。焊接是修复上述局部缺陷的主流方法,其中钨极惰性气体保护(TIG)焊因具有焊接质量高、焊接过程稳定和成本低等优点成为常用方法[4]。目前,有关304L不锈钢TIG焊接的研究主要集中在对接焊和堆焊修复方面。研究[5-6]发现,过高的热输入会使304L不锈钢TIG对接接头的显微硬度降低,力学性能下降。HU等[7]研究发现,单层多道TIG堆焊层内部存在气孔及多处未熔合缺陷。在采用对接焊或堆焊修复板材局部缺陷时,修复区域的热量较集中,易引起该区域组织粗化、性能劣化,并因较高的残余应力而产生新的焊接缺陷。补强板焊接通过将补强板覆盖于待修复板材(底板)缺陷区域,可有效分散热量,避免板材性能劣化。然而,TIG焊存在焊缝熔深浅、熔透能力有限的问题[8],容易导致补强板边缘与母材的连接强度不足,降低修复质量。在焊接过程中对焊枪引入周期性摆动,可以优化熔池流动与焊缝形貌,细化晶粒,从而提升接头力学性能[9]。针对补强板的TIG焊,焊枪摆动幅度是摆动TIG焊接中最关键的工艺参数之一,其通过改变电弧作用区域和熔池动力学行为,对焊缝成形、缺陷控制及力学性能产生系统性影响。为此,作者采用自动TIG焊结合摆动焊接技术,在不同焊枪摆动幅度下对304L不锈钢进行补强板焊接试验,研究了焊枪摆动幅度对接头组织和性能的影响,拟为核电用不锈钢补强板修复提供技术参考。

1 试样制备与试验方法

母材为304L不锈钢底板和补强板,补强板形状与尺寸如图1所示,焊接材料为直径1 mm的ER316L焊丝,母材和焊丝的化学成分如表1所示。

按图2所示将补强板置于待修复底板的缺陷位置上方,采用自制自动TIG焊接设备,将焊枪定位至补板上选定的某一斜边中点,向中心两侧进行周期性摆动施焊,摆动幅度分别为2,3,4 mm,焊接保护气体为纯度99.99%的氩气,流量为20 L·min^{-1},焊接电流为140 A,送丝速度为20 mm·s^{-1},焊接速度为100 mm·min^{-1},摆动速度为4 mm·s^{-1}。

收稿日期:2024-10-30;**修订日期**:2025-06-17
基金项目:国家自然科学基金联合基金重点支持项目(U22B20127);北京市科技计划重点项目(KZ202210017023);北京市属高等学校高水平科研创新团队建设支持计划项目(BPHR20220110);北京市教委一般科技项目(Z2023-007)
作者简介:朱加雷(1981—),男,山东菏泽人,教授,博士

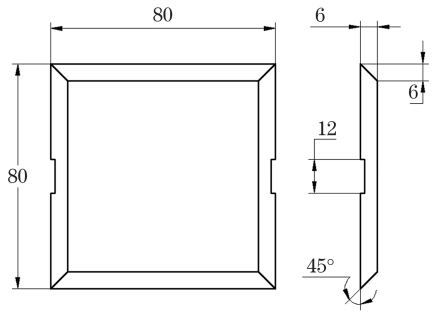

图1　补强板形状与尺寸

Fig. 1　Shape and size of patch plate

表1　304L不锈钢和ER316L焊丝的化学成分

Table 1　Chemical composition of 304L stainless steel and ER316L welding wire

材料	质量分数/%							
	C	Si	Mn	Cr	Ni	Mo	N	Fe
304L不锈钢	0.028	0.45	1.61	18.28	8.12	0.13	0.044	余
ER316L焊丝	0.027	0.56	1.69	18.30	11.21	2.10	0.039	余

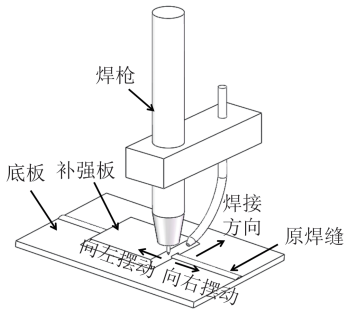

图2　焊接过程示意

Fig. 2　Welding process schematic

焊接完成后，采用线切割垂直于焊缝方向截取尺寸为10 mm×10 mm×15 mm的金相试样，经打磨、抛光后进行腐蚀处理，采用Leica-DMi8c型光学显微镜观察显微组织。采用D8 FOCUS型X射线衍射仪(XRD)进行物相组成分析，采用铜靶K_α射线，扫描速率为10 (°)·min^{-1}，扫描范围为20°～90°，工作电压为40 kV，工作电流为40 mA。采用HVS-1000Z型维氏硬度计测试焊缝中心显微硬度，载荷为9.8 N，保载时间为10 s，测点间距为0.3 mm，测至少3个点取平均值。在焊缝上截取尺寸为10 mm×10 mm×15 mm的试样，采用Versa STAT 3F型电化学工作站进行电化学试验，以饱和甘汞(SCE)电极为参照电极，铂电极为辅助电极，试样为工作电极，腐蚀介质为质量分数3.5%NaCl溶液，通过测量电化学阻抗谱(EIS)和极化曲线评估耐腐蚀性能。

2　试验结果与讨论

2.1　物相组成

由图3可以看出，不同摆动幅度下接头焊缝中均检测到γ相(111)、(200)、(220)晶面衍射峰和δ相(110)晶面衍射峰。随着摆动幅度增加，γ相(111)晶面的衍射峰强度减弱，δ相(110)晶面的衍射峰强度增加，说明γ-奥氏体含量减少而δ-铁素体含量增加，推测是因为摆动幅度增加使冷却速率增大，δ-铁素体相变过程受到抑制。随着摆动幅度增加，γ相(111)晶面衍射峰半高宽增大，说明γ-奥氏体晶粒尺寸有所减小[10]。

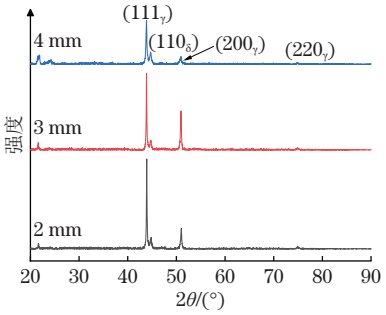

图3　不同摆动幅度下接头焊缝的XRD谱

Fig. 3　XRD patterns of weld seam of joint under different swing amplitudes

2.2　显微组织

由图4可知，不同摆动幅度下焊缝和熔合区组织均由γ-奥氏体和δ-铁素体组成，符合铁素体-奥氏体凝固模式特征：熔池凝固初期，δ-铁素体优先析出，随后部分转变成γ-奥氏体，形成两相混合组织[11-12]。当摆动幅度较低(2 mm)时，焊缝冷却相对缓慢，δ-铁素体相变相对充分，短小枝状的残留铁素体之间形成粗大的奥氏体晶粒，γ-奥氏体含量较高；随着摆动幅度增加，由于δ-铁素体相变受到抑制，δ-铁素体含量增多，奥氏体含量减少且晶粒显著细化。奥氏体晶粒显著细化是因为随着摆动幅度增大，焊缝熔宽增加，在焊接速度恒定条件下，焊缝冷却速率增大，导致形核率增加[13]。当摆动幅度大于2 mm时，焊缝中未完全转变的δ-铁素体以骨架状沿γ-奥氏体柱状晶/等轴晶的晶界分布。相较于焊缝，熔合区奥氏体晶粒更细小，铁素体含量更多，这是因为熔合区靠近母材，冷却速率大于焊缝，δ-铁素体扩散受阻，呈条状贯穿γ-奥氏体晶粒。随着摆动幅度增大，熔合区冷却速率增大，晶粒细化明显。

2.3　显微硬度

当摆动幅度为2，3，4 mm时，接头焊缝的显微

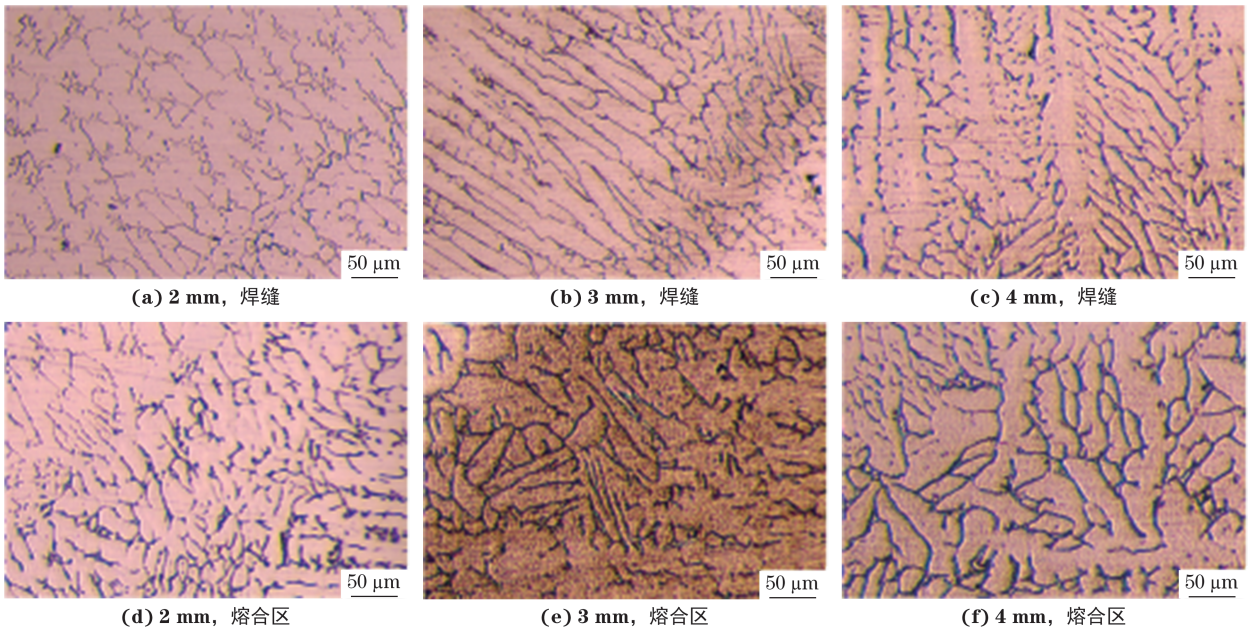

(a) 2 mm，焊缝　(b) 3 mm，焊缝　(c) 4 mm，焊缝

(d) 2 mm，熔合区　(e) 3 mm，熔合区　(f) 4 mm，熔合区

图 4　不同摆动幅度下接头焊缝和熔合区的显微组织

Fig. 4　Microstructures of weld seam (a–c) and fusion zone (d–f) of joint under different swing amplitudes

硬度分别为154，159，163 HV；随着摆动幅度增加，焊缝显微硬度提高。这是因为随着摆动幅度增大，晶粒细化，晶界面积增大，阻碍位错运动能力增强，抵抗塑性变形能力提高，显微硬度提升[14]；快速冷却还会抑制δ-铁素体向γ-奥氏体的相变，保留在组织中的δ-铁素体含量增多，而δ-铁素体层错能较高，因此硬度提高[15-16]。

2.4　耐腐蚀性能

由图5可知，随着摆动幅度增大，接头焊缝的容抗弧半径减小，说明焊缝的抗腐蚀能力减弱[17]。利用切线交点法对极化曲线进行拟合，得到当摆动幅度为2，3，4 mm时，焊缝的自腐蚀电位分别为－102.1，－210.404，－211.648 mV，自腐蚀电流密度分别为0.795，2.825，1.117×10^{3} nA·cm^{-2}。可知随着摆动幅度增大，腐蚀速率加快，接头焊缝的耐腐蚀性能减弱。摆动幅度2 mm条件下焊缝中的奥氏体含量较高，而奥氏体组织具有较好的耐腐蚀性能[18]，因此该条件下焊缝耐腐蚀性能更优。

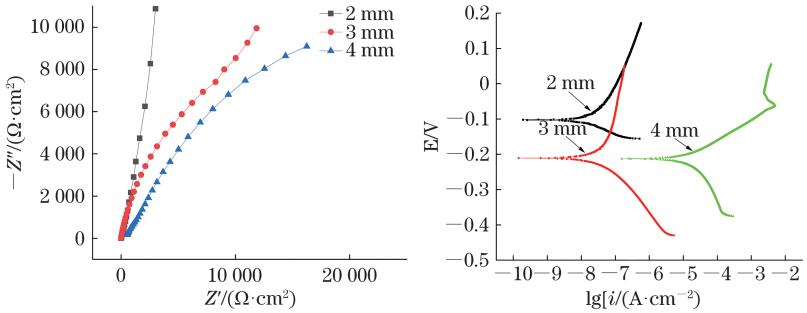

(a) 电化学阻抗谱　(b) 极化曲线

图 5　不同摆动幅度下接头焊缝的电化学阻抗谱和极化曲线

Fig. 5　Electrochemical impedance spectroscopy (a) and polarization curves (b) of weld seam of joint under different swing amplitudes

3　结　论

（1）不同摆动幅度(2，3，4 mm)下接头焊缝组织主要为γ-奥氏体＋δ-铁素体。随着摆动幅度增加，γ相(111)晶面衍射峰强度降低，半高宽增加，δ相(110)晶面衍射峰强度增加，较大摆动幅度(3，4 mm)下δ-铁素体以骨架状沿γ-奥氏体柱状晶/等轴晶的晶界分布。

（2）随着摆动幅度增加，由于δ-铁素体含量增加、γ-奥氏体含量减少且晶粒细化，接头焊缝的显微硬度提高，焊缝的自腐蚀电位减小，自腐蚀电流密度增大，耐腐蚀性能下降。

参考文献：

[1]　陈越. 脉冲电流处理参数对304不锈钢微观组织的影

响[D]. 沈阳：东北大学，2019.
CHEN Y. Effect of pulse current parameters on microstructure of 304 stainless steel[D]. Shenyang: Northeastern University, 2019.

[2] 王文军，龚五堂. 304不锈钢激光焊接工艺及微观组织研究[J]. 应用激光，2018，38(2)：245-249.
WANG W J, GONG W T. Study on laser welding process and microstructure of 304 stainless steel[J]. Applied Laser, 2018, 38(2): 245-249.

[3] KURYNTSEV S V, GILMUTDINOV A K. Welding of stainless steel using defocused laser beam[J]. Journal of Constructional Steel Research, 2015, 114: 305-313.

[4] 崔丽，朱学军，栗卓新. 不锈钢薄板高速钨极氩弧焊的研究[J]. 热加工工艺，2005，34(4)：22-24.
CUI L, ZHU X J, LI Z X. Study of high speed GTAW process for thin-plate stainless steel[J]. Hot Working Technology, 2005, 34(4): 22-24.

[5] ROY A, GHOSH N, MONDAL S. Effect of heat input on mechanical and metallurgical properties of AISI 304L stainless steel by using TIG welding[J]. Welding International, 2023, 37(2): 91-100.

[6] KUMAR P, SINHA A N, HIRWANI C K, et al. Effect of welding current in TIG welding 304L steel on temperature distribution, microstructure and mechanical properties[J]. Journal of the Brazilian Society of Mechanical Sciences and Engineering, 2021, 43(7): 369.

[7] HU C Y, LI H L, LIU X Q, et al. Investigation on microstructure and properties of the local dry underwater TIG welding of 304L stainless steel[J]. Materials Today Communications, 2025, 44: 111978.

[8] 曹润平，王克勇，齐勇田. 316L不锈钢PAW-TIG复合焊接的研究[J]. 兵器材料科学与工程，2019，42(6)：29-33.
CAO R P, WANG K Y, QI Y T. Hybrid PAW-TIG welding technology of 316L stainless steel[J]. Ordnance Material Science and Engineering, 2019, 42(6): 29-33.

[9] 牛虎山，林化强，崔洪芝. 6005A铝合金摆动激光焊接组织及力学性能研究[J]. 精密成形工程，2023，15(4)：33-39.
NIU H S, LIN H Q, CUI H Z. Microstructure and mechanical properties of 6005A aluminum alloy by oscillat-ing laser welding[J]. Journal of Netshape Forming Engineering, 2023, 15(4): 33-39.

[10] 任超，罗军明，陈宇海，等. 喷丸对TC4合金微弧氧化涂层磨损和腐蚀行为的影响[J]. 材料导报，2020，34(9)：18081-18085.
REN C, LUO J M, CHEN Y H, et al. Effect of shot peening on wear and corrosion behavior of micro-arc oxidation coating of TC4 alloy[J]. Materials Reports, 2020, 34(9): 18081-18085.

[11] LIANG G, WAN C, WU J, et al. In situ observation of growth behavior and morphology of delta-ferrite as function of solidification rate in an AISI304 stainless steel[J]. Acta Metallurgica Sinica(English Letters), 2006, 19(6): 441-448.

[12] 周琴. 激光增材制造316不锈钢凝固模式与显微组织的研究[D]. 长沙：湖南大学，2021.
ZHOU Q. Study on solidification mode and microstructure of 316 stainless steel by laser additive manufacturing[D]. Changsha: Hunan University, 2021.

[13] WEI Y S, WANG C, YOU J, et al. Substantial grain refinement of Al-Mn-Si alloys mediated by collaborative effect of Al-5Ti-1B refiner and sub-rapid solidification[J]. Journal of Materials Science & Technology, 2024, 187: 230-239.

[14] 陈俊科，石岩，刘佳，等. 奥氏体不锈钢激光焊接工艺研究[J]. 应用激光，2015，35(3)：335-338.
CHEN J K, SHI Y, LIU J, et al. A study of austenitic stainless steel laser welding process[J]. Applied Laser, 2015, 35(3): 335-338.

[15] 赵友亮，朱加雷，赵晓鑫，等. 空气和水下环境304L不锈钢密封堆焊工艺对比[J]. 中国表面工程，2024，37(4)：280-290.
ZHAO Y L, ZHU J L, ZHAO X X, et al. Comparison of 304L stainless steel sealing overlay welding processes in air and underwater environments[J]. China Surface Engineering, 2024, 37(4): 280-290.

[16] EGHLIMI A, SHAMANIAN M, ESKANDARIAN M, et al. Evaluation of microstructure and texture across the welded interface of super duplex stainless steel and high strength low alloy steel[J]. Surface and Coatings Technology, 2015, 264: 150-162.

[17] 朱东芳，朱加雷，焦向东，等. 921A钢激光-MAG复合焊接头组织及性能[J]. 焊接，2022(9)：25-29.
ZHU D F, ZHU J L, JIAO X D, et al. Microstructure and mechanical properties of 921A steel welded joint by laser-MAG hybrid welding[J]. Welding & Joining, 2022(9): 25-29.

[18] 耿真真，张钰柱，杜小将，等. S^{2-}和Cl^{-}对316L奥氏体不锈钢的腐蚀钝化行为的协同作用[J]. 中国腐蚀与防护学报，2024，44(3)：797-806.
GENG Z Z, ZHANG Y Z, DU X J, et al. Synergistic effect of S^{2-} and Cl^{-} on corrosion and passivation behavior of 316L austenitic stainless steel[J]. Journal of Chinese Society for Corrosion and Protection, 2024, 44(3): 797-806.

（下转第107页）

Hot Deformation Behavior and Constitutive Model of Forged 304L Austenitic Stainless Steel

HUANG Jian, PANG Zongxu, ZHANG Jianping, WANG Yong, WANG Tie, ZHOU Bo

(State Key Laboratory of Metallic Materials for Marine Equipment and Applications, Iron & Steel Research Institutes of Ansteel Group Corporation, Anshan 114009, China)

Abstract: Single-pass isothermal compression tests (compression to true strain of 0.69) were conducted on forged 304L austenitic stainless steel with a thermal simulation equipment at different deformation temperatures (900–1 200 ℃) and different strain rates (0.01–10 s^{-1}), and the hot deformation behavior was studied. The strain compensated Arrhenius model and modified Johnson-Cook (JC) model considering deformation temperature, strain rate and true strain were established for test steel compression, and the prediction accuracy of the two models was compared. The results show that with the increase of deformation temperature, the dynamic recrystallization of test steel became more complete, and was basically complete when the deformation temperature was 1 200 ℃, with the formation of many twins. At the deformation temperature of 900–1050 ℃ and the strain rate of 1,5 s^{-1}, the flow stress tended be stable after the strain increased to a certain value due to the synergistic effect of dynamic recrystallization and dynamic recovery. At the deformation temperature of 900–1 200 ℃ and the deformation rate of 0.01, 0.1, 10 s^{-1} and at the deformation temperature of 1 100–1 200 ℃ and the deformation rate of 1,5 s^{-1}, with the increase of strain, the flow stress increased first, reached the peak value and then decreased,showing the characteristics of dynamic recrystallization type. The absolute values of average relative errors of the flow stress predicted by the strain compensated Arrhenius model and the modified JC model and test results were 4.916% and 7.648%, and the correlation coefficients were 0.993 41 and 0.985 24, respectively; the prediction accuracy of the strain compensated Arrhenius model was higher.

Key words: 304L austenitic stainless steel; hot deformation; Johnson-Cook constitutive model; strain-compensated Arrhenius model; microstructure

（上接第18页）

Influence of Welding Torch Swing Amplitude on Microstructure and Properties of TIG Welded Jiont of 304L Stainless Steel Patch Plate

ZHU Jialei[1], ZHU Wenlei[1], JIAO Xiangdong[1], LI Shougen[1], GUO Fangtao[1], ZHANG Hongtao[2]

(1. School of Mechanical Engineering, Beijing Institute of Petrochemical Technology, Beijing 102617, China;
2. School of Materials Science and Engineering, Harbin Institute of Technology (Weihai), Weihai 264209, China)

Abstract: A patch plate welding test was carried out on 304L stainless steel by acctomatic tungsten inert gas (TIG) welding combined with swing welding under different swing amplitudes (2, 3, 4 mm) with ER316L welding wires. The influence of welding torch swing amplitude on the microstructure, phase composition, microhardness, and corrosion resistance of weld seam of the joint was investigated. The results show that the microstructure of weld seam of the joint under different swing amplitudes was mainly composed of γ-austenite and δ-ferrite. With the increase of swing amplitude, the diffraction peak intensity of (111) crystal plane of γ phase decreased, and the diffraction peak intensity of (110) crystal plane of δ phase increased. Under large swing amplitudes (3, 4 mm), the δ-ferrite was distributed in a skeletal shape along the grain boundaries of the γ-austenite columnar crystal/equiaxed crystal. With the increase of swing amplitude, the content of δ-ferrite increased, the content of γ-austenite decreased and the grains of γ-austenite were refined, resulting in the increase of hardness of weld seam, the decrease of self corrosion potential, the increase of self corrosion current density, and the decrease of corrosion resistance.

Key words: tungsten inert gas welding; swing welding; 304L stainless steel; microstructure; electrochemical corrosion